

Article

Optimal Sizing Procedure for Electric Vehicle Supply Infrastructure Based on DC Microgrid with Station Commitment

Benedetto Aluisio, Maria Dicorato *, Imma Ferrini, Giuseppe Forte, Roberto Sbrizzai and Michele Trovato

Department of Electrical and Information Engineering, Politecnico di Bari, via E. Orabona, 4, 70125 Bari, Italy; benedetto.aluisio@poliba.it (B.A.); i.ferrini@studenti.poliba.it (I.F.); giuseppe.forte83@gmail.com (G.F.); roberto.sbrizzai@poliba.it (R.S.); micheleantonio.trovato@poliba.it (M.T.)

* Correspondence: maria.dicorato@poliba.it

Received: 21 March 2019; Accepted: 5 May 2019; Published: 18 May 2019



Abstract: The diffusion of electric vehicles (EVs) can be sustained by the presence of integrated solutions offering parking and clean power supply. The recourse to DC systems allows better integration of EV bidirectional energy exchange, photovoltaic panels, and energy storage. In this paper, a methodology for optimal techno-economic sizing of a DC-microgrid for covering EV mobility needs is carried out. It is based on the definition of different scenarios of operation, according to typical EV usage outlooks and environmental conditions. In each scenario, optimal operation is carried out by means of a specific approach for EV commitment on different stations. The sizing procedure is able to handle the modular structure of microgrid devices. The proposed approach is applied to a case study of an envisaged EV service fleet for the Bari port authority.

Keywords: DC microgrid; electric vehicles; optimal sizing; station commitment

1. Introduction

The spreading of electric vehicles (EVs) can represent a powerful means to cope with mobility needs and realize a diversification of transport energy use with a lower carbon footprint [1]. In order to bolster the diffusion of EVs among end-users (e.g., residential, commuters, company fleets), along with selling price reduction, the presence of charging stations represents the most remarkable aspect [2]. However, to avoid demand peaks given by the presence of several EVs at the same time (e.g., at work arrival, or at homecoming), the charge process should be planned, supervised, and controlled through a smart charging strategy, as described in [3,4]. The exploitation of vehicle-to-grid (V2G) is useful to cope with this necessity, where the EVs can act as a mobile energy storage device and even feed one another, implementing vehicle-to-vehicle exchanges as envisaged by [5].

Photovoltaic (PV) technology is particularly suitable for integration with EV charging stations, as reviewed in [6]. A specific realization is obtained by canopies able to host PV panels and provide for shaded vehicle parking, as proposed by [7], whereas, in [8] an analysis on different utilization cases of this system in urban contexts is reported. The integration of PV and EV charging station has been proposed in several works, e.g., charge/discharge models of EVs in the presence of PV are analysed in [9], and in [10] economic models are developed for EV and parking owner perspectives under parking fee policies. Effects on regional basis are analysed in [11]. In order to reduce the EV impact on the network, the integration of energy storage systems (ESS) in EV charging stations can be useful [12], with the aim of shifting power exchange according to price signals, smoothing out time variations [13]. Moreover, smart EV charging points, even integrated in microgrids, can contribute to

attaining automation goals of power system structural controllability by proper placement [14] and can take part to monitoring and control structure of distribution networks [15].

The integration of those elements (EVs, charging points with V2G, PV systems, ESS) can constitute an Electric Vehicle Supply Infrastructure (EVSI) with a microgrid outline. This structure, introduced in previous works [16,17], can reveal particular suitability for managing a fleet of corporate EVs, for instance in a small/medium enterprise or in a public entity. Moreover, all the mentioned EVSI components can be directly integrated in a DC-microgrid architecture, reducing AC/DC converter employment, as described in the reviews [18,19]. In this context, proper control strategies should be implemented involving smart charging individuating operation modes of converters as in [20,21], as well as real-time control and robust islanding [22,23].

A research activity is open on the integration of EV-based microgrid, and operation planning strategies are investigated with minimum total cost goal under different vehicle behaviors in [24], whereas the cost of energy circulation in storage system is added in [25]. However, since the investment in EVs and relevant charging systems is still a major concern, a particular care is devoted to the sizing of an EV-based microgrid. This problem has been faced combining PV and EVs in [20], and considering the presence of a single ESS and EVs in [26] where network limits are studied and cost items are detailed for AC and DC configurations. Moreover, in [27] optimal sizing is determined and investment cost sensitivity is analysed, in [28] design criteria are discussed for a fast charging station with ESS and PV for an EV fleet and the operation is tested over a week, and in [29] optimal sizing including probabilistic solar production and queueing model of EVs is carried out.

In this paper, a procedure for techno-economic evaluation for DC microgrid configuration of EVSI is carried out. The procedure is intended to reduce economical efforts for investment and lifetime management of the microgrid. In particular, realistic spatial and technical limitations are taken into account, along with different operating conditions based on EV needs and availability of non-programmable renewable sources. The analysed configuration involves feasible combinations of converters as well as modular PV panels, ESS elements, and EV charging stations, with a proper interface with the low-voltage AC distribution network. The proposed procedure is applied to the sizing of the microgrid that will be realized in the area of the Bari Port Authority (Italy).

The main contributions of the paper with respect to the existing literature can be individuated as follows:

- A mixed-integer procedure for EV-based microgrid optimal sizing and operation is provided, to cope with the modularity of microgrid components;
- The individuation of utilization scenarios, according to weather conditions and envisaged EV uses, is adopted, and discounted investment and operation costs are included;
- A specific EV commitment is developed, in order to plan the station to which each EV should be connected;
- In order to draw the influence of DC microgrid layout, an accurate configuration is analysed on a realistic test case.

The paper is organized as follows. In Section 2, the proposed DC microgrid configurations are illustrated, and the formulation of the proposed methodology for DC microgrid optimal sizing and operation is described. In Section 3, the input data for the test case are presented. Simulation results are illustrated and discussed in Section 4. Conclusions are reported in Section 5.

2. DC Microgrid Optimal Sizing Methodology

For the complete list of symbols and their meaning, please refer to the Nomenclature at the end of the paper.

2.1. DC Microgrid Configurations

In order to carry out the sizing procedure, the proposed configurations for the DC microgrid of the EVSI are considered. The configuration, briefly discussed in [17], is depicted in Figure 1. It involves a bidirectional AC/DC converter for grid connection at Point of Common Coupling (PCC), monodirectional DC/DC converter with MPPT functionality for the integration of the PV system, a bidirectional DC/DC converter for the ESS, and different bidirectional DC/DC converters for the EV charging stations, in order to enable V2G performances. All the converters, including relevant protection devices, are connected to a common DC busbar at a proper voltage level. Moreover, suitable internal collection systems for the input of PV panel strings to the converter and for the ESS modules are provided.

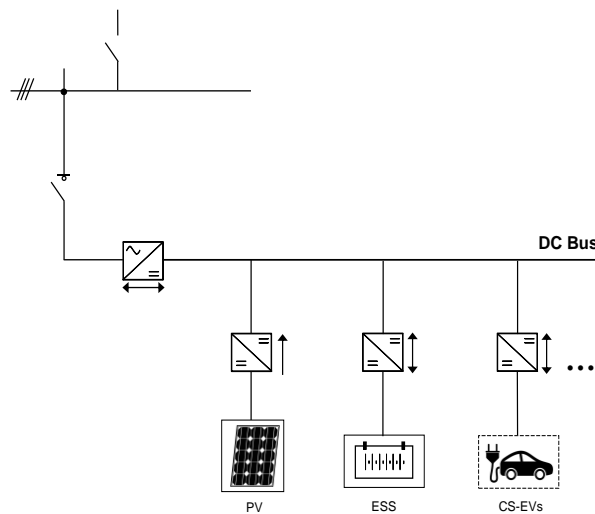


Figure 1. Configuration for the DC-based microgrid.

2.2. Modeling of EVSI Components

The EVSI can include N_p PV technologies and N_i ESS technologies, and is able to exchange power with N_j EVs through N_k stations, where a set of N_r standards can be chosen. The behavior of each component is described by proper models for each t -th time step in the s -th scenario.

In order to assess the operation of the microgrid in the presence of different frameworks for vehicle use and generation availability, a scenario-based procedure is considered, analogously to analysis carried out in different contexts of renewable-storage coupling in [30] and in photovoltaic-based nanogrid reliability analysis in [31]. Since solar power production depends on weather conditions and seasons, and storage devices and EVs can show different use in weekdays as well as in subperiods of the year, a certain number N_s of scenarios, i.e., typical days, are defined in advance, considering that each s -th scenario can be observed for a given number of times D_s during the year. Moreover, due to the limited dimensions of the microgrids, the sizing procedure accounts for power and energy aspects, leaving voltage control to the implementation stage close to real time, even if operation under different scenarios is accounted for.

2.2.1. PV Systems

The power output of the p -th PV system depends on the available solar radiation $G_{p,s,t}$, installed PV power R_p and technological features, by means of the following expression:

$$P_{p,s,t} = R_p \cdot \frac{\eta_{p,s,t} \cdot G_{p,s,t}}{\eta_p^{std}} \quad (1)$$

In (1), the efficiency of the p -th PV system, $\eta_{p,s,t}$, is related to the forecasted weather conditions of the specific time step (i.e., solar radiation and ambient temperature $\vartheta_{s,t}$) as follows [18]:

$$\eta_{p,s,t} = \eta_p^{std} \cdot \left[1 - a_p \cdot \left(\vartheta_{s,t} + G_{p,s,t} \cdot \frac{\vartheta_p - \vartheta_p^{NOCT}}{G_p^{NOCT}} - \vartheta_p^{std} \right) \right] \quad (2)$$

where η_p^{std} is the efficiency level at standard conditions (incident radiation 1 kW/m², temperature $\vartheta_p^{std} = 25$ °C) and a_p is the power coefficient p -th PV system. Moreover, the temperature variation from nominal operating conditions (with reference temperature $\vartheta_p^{NOCT} = 20$ °C and reference radiation $G_p^{NOCT} = 0.8$ kW/m²) is related to the normal operating temperature of the PV cell ϑ_p . These data can be easily taken from PV panel datasheets.

Since the relation (1) linearly links power output with the installed power R_p according to solar radiation $G_{p,s,t}$, $P_{p,s,t}$ is not included in state variables. The incident solar radiation $G_{p,s,t}$ is estimated with a proper model based on the determination of direct, diffuse, and reflected radiation according to the day, the time of the day, and the PV panel orientation, starting from total radiation forecast on horizontal plane [32].

The PV installation R_p is limited by available surface of parking roofs S^{tot} and should ensure shadowing for all the parking places next to EV charging stations, each requiring an area S_k :

$$\sum_{k \in \Omega_k} S_k \leq \sum_{p \in \Omega_p} \frac{R_p}{\eta_p^{std}} \leq S^{tot} \quad (3)$$

Moreover, since the PV system is made up by discrete modules, the installed power of the p -th PV technology to the number n_p of PV modules, according to the unit power of the module M_p , by the following equality constraint:

$$R_p = n_p \cdot M_p \quad (4)$$

Finally, the size of PV converter should be not less than the installed power of the PV system, and only one converter per each PV technology has to be installed. Converter sizes W_m are determined in order to comply with voltage range variation of PV panel strings under temperature variations.

$$P_{p,s,t} \leq \sum_{m \in \Omega_m} W_m \cdot b_{m,p} \quad (5)$$

$$\sum_{m \in \Omega_m} b_{m,p} \leq 1 \quad (6)$$

2.2.2. Energy Storage Systems

The behavior of ESSs is characterized by the energy amount present in the storage device in each time step. However, a high degree of correspondence is observed between energy amount and state-of-charge (SOC), given by the levels of current [33]. The assumption of discarding voltage variations in this procedure further leads to the exploitation of SOC in each time step $E_{i,s,t}$ to define ESS availability in the operation planning [25].

SOC variation over the time step duration Δt is due to charging/discharging process, with power levels $P_{i,s,t}^c$ or $P_{i,s,t}^d$, by proper charge and discharge efficiencies, η_i^c and η_i^d . The following relation holds for the t -th time step:

$$E_{i,s,t} = E_{i,s,t-1} + \Delta t \cdot \left(\eta_i^c \cdot P_{i,s,t}^c - \frac{P_{i,s,t}^d}{\eta_i^d} \right) - z_i \cdot R_i \quad (7)$$

where $E_{i,s,t-1}$ represents the SOC of the i -th ESS in the previous time step of the s -th scenario. For $t = 1$, $E_{i,s,0}$ represents the imposed SOC initial condition. The last term in (7) refers to self-discharge,

as a quota z_i of installed amount R_i . Moreover, the SOC at $t = Nt$ is imposed equal to the initial condition, allowing replication of the behavior for consecutive days:

$$E_{i,s,Nt} = E_{i,s,0} \quad (8)$$

Technical limits of the i -th ESS are accounted by means of constraints on charge power, discharge power, and SOC, depending on installed amount R_i by means of energy-to-power ratios in charge and discharge, φ_i^c and φ_i^d , and maximum/minimum SOC levels, \underline{e}_i and \bar{e}_i :

$$0 \leq P_{i,s,t}^c \leq \frac{R_i}{\varphi_i^c} \cdot b_{i,s,t} \quad (9)$$

$$0 \leq P_{i,s,t}^d \leq \frac{R_i}{\varphi_i^d} \cdot (1 - b_{i,s,t}) \quad (10)$$

$$\underline{e}_i \cdot R_i \leq E_{i,s,t} \leq \bar{e}_i \cdot R_i \quad (11)$$

The total installation of ESSs is limited by available volume V^{tot} for hosting the devices:

$$\sum_{i \in \Omega_i} \delta_i \cdot R_i \leq V^{tot} \quad (12)$$

Analogously to PV system, the following equality constraints link the installed size of the i -th ESS to the number n_i of modules, according to the unit size of the chosen battery M_i , and to the size of the converter:

$$R_i = n_i \cdot M_i \quad (13)$$

$$R_i \leq \sum_{h \in \Omega_h} W_h \cdot \varphi_i^d \cdot b_{h,i} \quad (14)$$

$$\sum_{h \in \Omega_h} b_{h,i} \leq 1 \quad (15)$$

2.2.3. Electric Vehicles and Stations

EVs are dealt with as storage devices, as long as they are connected to a station. The relation for SOC update is valid for the t -th time step between $\tau_{j,s}^A + 1$ and $\tau_{j,s}^L$:

$$E_{j,s,t} = E_{j,s,t-1} + \Delta t \cdot \left(\rho_j^c \cdot P_{j,s,t}^c - \frac{P_{j,s,t}^d}{\rho_j^d} \right) \quad (16)$$

where, at $t = \tau_{j,s}^A + 1$, $E_{j,s,t-1} = E_{j,s}^A$, as the initial SOC condition at EV arrival, whereas at $t = \tau_{j,s}^L$, $E_{j,s,t} = E_{j,s}^L$ the final desired SOC level at EV leaving. It should be remarked that this formulation is based on the assumption that each EV is parked for one interval per day. In the case the daily EV usage pattern includes two (or more) parking intervals, it is dealt with as two (or more) virtual EVs with a single parking interval.

Technical limits of the j -th EV, valid during parking interval, involve constraints on power levels, capped by charge and discharge limits \bar{P}_j^c and \bar{P}_j^d , and on SOC and power levels:

$$0 \leq P_{j,s,t}^c \leq \bar{P}_j^c \cdot b_{j,s,t} \quad (17)$$

$$0 \leq P_{j,s,t}^d \leq \bar{P}_j^d \cdot (1 - b_{j,s,t}) \quad (18)$$

$$\underline{v}_j \leq E_{j,s,t} \leq \bar{v}_j \quad (19)$$

As regards technologies for charging stations, the following relations (20)–(21) link maximum charge/discharge power of the k -th station, \bar{P}_k^c and \bar{P}_k^d respectively, to the power exchange levels admitted by the r -th technology, Ψ_r^c and Ψ_r^d , whereas the association of the r -th technology to the k -th station is ensured by (22). It should be noted that the case where the r -th EV station standard would not provide for V2G is modelled by $\Psi_r^d = 0$:

$$\bar{P}_k^c = \sum_{r \in \Omega_r} b_{r,k} \cdot \Psi_r^c \quad (20)$$

$$\bar{P}_k^d = \sum_{r \in \Omega_r} b_{r,k} \cdot \Psi_r^d \quad (21)$$

$$\sum_{r \in \Omega_r} b_{r,k} = 1 \quad (22)$$

2.2.4. Electric Vehicles Station Commitment

The electric vehicle commitment is aimed at scheduling the station at which each EV should be connected, creating a link between their features.

In the planning stage, the number of stations Nk to be included in the EVSI is evaluated. For each time step of each scenario, the number of parked vehicles $J_{s,t}$ is determined starting from information on $\tau_{j,s}^A$ and $\tau_{j,s}^L$. Therefore, for each scenario, the maximum number of EVs parked at the same time is obtained, and the relevant time interval is individuated:

$$\bar{J}_s = \max_t (J_{s,t}) \quad (23)$$

$$\bar{\tau}_s = t J_{s,t} = \bar{J}_s \quad (24)$$

The number of EV stations is eventually set to the minimum necessary to cover the maximum amount of EVs parked at the same time in any scenario:

$$Nk = \max_s \bar{J}_s \quad (25)$$

Moreover, EV exploitation is characterized by evaluating, for each EV in each scenario, the average power needed to reach the final state $\pi_{j,s}$:

$$\pi_{j,s} = \frac{|E_{j,s}^L - E_{j,s}^A|}{\tau_{j,s}^L - \tau_{j,s}^A} \quad (26)$$

Once Nk is determined, for each scenario, the EV commitment starts from the time step $\bar{\tau}_s$. The \bar{J}_s EVs parked in this time step are associated to the charging stations according to a list sorted according to the index $\pi_{j,s}$: the EV with the highest index is connected to the first station, $k = 1$, and so on.

After that, the remaining $Nj - \bar{J}_s$ EVs are ordered according to the power index $\pi_{j,s}$. For each EV in this ranking, starting from the first one, the procedure tries the connection to the first available station, avoiding time superposition with the EVs previously selected.

This procedure can leave in idle state the last stations. In this way, the binary parameter $\beta_{j,k,s}$ is determined for all EVs, stations, and scenarios.

For purpose of exemplification, an application of the EV station commitment procedure is reported in Appendix A.

Therefore, the amount of charge and discharge power that the j -th EV can exchange depends not only on the EV features, but also on the k -th station it is connected to in the s -th scenario, as follows:

$$0 \leq P_{j,s,t}^c \leq \bar{P}_k^c \cdot \beta_{j,k,s} \quad (27)$$

$$0 \leq P_{j,s,t}^d \leq \bar{P}_k^d \cdot \beta_{j,k,s} \quad (28)$$

2.2.5. Microgrid Balance and Power Exchanges

The overall behaviour of the microgrid is governed by power balance relation, where the generation is represented by net PV production, ESS discharge, possible EV discharge, and grid withdrawal, whereas the load includes ESS and EV charge and grid power delivery. Due to limited dimensions, microgrid balance is expressed as a single-bus power balance, considering net power contributions at the DC bus by means of converter efficiency for each device (reducing generation and increasing the load), as reported in (29):

$$\sum_{p \in \Omega_p} \zeta^M \cdot P_{p,s,t} + \sum_{i \in \Omega_i} \zeta^H \cdot P_{i,s,t}^d + \sum_{j \in \Omega_j} \zeta^K \cdot P_{j,s,t}^d + \zeta^F \cdot P_{s,t}^w = \sum_{i \in \Omega_i} \frac{1}{\zeta^H} \cdot P_{i,s,t}^c + \sum_{j \in \Omega_j} \frac{1}{\zeta^K} \cdot P_{j,s,t}^c + \frac{1}{\zeta^F} \cdot P_{s,t}^g \quad (29)$$

The power exchange across the interfacing converter should withstand specific constraints related to the installed converter size R^F , as reported in relations (30)–(31):

$$R^F = \sum_{f \in \Omega_f} W_f \cdot b_f \quad (30)$$

$$\sum_{f \in \Omega_f} b_f = 1 \quad (31)$$

The power exchange of the DC microgrid with the AC distribution network, in injection $P_{s,t}^g$ or in absorption $P_{s,t}^w$ is limited by the following relations, avoiding contemporaneous withdrawal and injection by means of the binary variable $b_{s,t}^g$:

$$0 \leq P_{s,t}^g \leq \bar{P}^g \cdot b_{s,t}^g \quad (32)$$

$$0 \leq P_{s,t}^w \leq \bar{P}^g \cdot (1 - b_{s,t}^g) \quad (33)$$

where \bar{P}^g is a conveniently high value.

Moreover, grid exchange levels are bounded by installed converter size R^F , therefore the following relations hold:

$$0 \leq P_{s,t}^g \leq R^F \quad (34)$$

$$0 \leq P_{s,t}^w \leq R^F \quad (35)$$

2.3. Objective and Procedure Formulation

The goal of DC microgrid optimal design under the EV exploitation conditions and space limitations is achieved by minimizing the total lifetime cost C_T of the EVSI:

$$C_T = C_B + C_O. \quad (36)$$

The lifetime operation cost C_O is determined by actualizing the yearly operation cost of the EVSI C_O^Y , determined by considering the occurrence of the s -th scenario for D_s times over one year, as follows:

$$C_O^Y = \sum_{s=1}^{Ns} D_s \cdot \sum_{t=1}^{Nt} \Delta t \cdot \left[q_{s,t}^{wv} \cdot P_{s,t}^w - \gamma_{s,t}^g \cdot P_{s,t}^g + \sum_{j \in \Omega_j} (q_{j,s,t} \cdot P_{j,s,t}^c + \gamma_{j,s,t} \cdot P_{j,s,t}^d) \right] \quad (37)$$

where the terms in square brackets include total cost for electricity purchase from AC network at unit cost $q_{s,t}^{wv}$, total income from power delivery to AC network at unit revenue $\gamma_{s,t}^g$, total degradation cost for EV charge at rate $q_{j,s,t}$, and for EV discharge at rate $\gamma_{j,s,t}$.

Assuming that the analyzed year replicates along all the lifetime, C_O is determined by discounting C_O^Y by the annuity factor:

$$C_O = \frac{1 - (1 + \alpha)^{-Ny}}{\alpha} \cdot C^y \quad (38)$$

The building cost C_B is determined as the sum of purchasing and installation costs associated to PVs C_B^P , ESSs C_B^I , EV stations C_B^K , and grid connections C_B^G , as follows:

$$C_B = C_B^P + C_B^I + C_B^K + C_B^G \quad (39)$$

The single contributions are determined by the following (40)–(43), respectively, exploiting unit costs for PV panels c_p and ESS modules c_i related to total size, whereas costs of PV converters c_m , ESS converters c_h , EV station technologies c_r , grid converter c_f , and AC grid connection c^g are linked to the values of binary variables for size selection.

$$C_B^P = \sum_{p \in \Omega_p} \left(c_p \cdot R_p + \sum_{m \in \Omega_m} c_m \cdot b_{m,p} \right) \quad (40)$$

$$C_B^I = \sum_{i \in \Omega_i} \left(c_i \cdot R_i + \sum_{h \in \Omega_h} c_h \cdot b_{h,i} \right) \quad (41)$$

$$C_B^K = \sum_{r \in \Omega_r} c_r \cdot \sum_{k \in \Omega_k} b_{r,k} \quad (42)$$

$$C_B^G = \sum_{f \in \Omega_f} (c_f + c^g) \cdot b_f \quad (43)$$

Microgrid optimal design problem can be synthesized in the following Mixed Integer Linear Programming formulation:

$$\begin{aligned} & \min C_T(\mathbf{x}) \\ & \text{s.t.} \begin{cases} g(\mathbf{x}) = 0 \\ h(\mathbf{x}) \leq 0 \\ \underline{\mathbf{x}} \leq \mathbf{x} \leq \bar{\mathbf{x}} \end{cases} \end{aligned} \quad (44)$$

where equalities $g(\mathbf{x}) = 0$, inequalities $h(\mathbf{x}) \leq 0$, and state variable limits $\underline{\mathbf{x}} \leq \mathbf{x} \leq \bar{\mathbf{x}}$ include the relations reported in Section 2.2.

3. Test System

The investigation is based on the expected installation of the proposed system in the area of the Bari Port Authority, Italy, where a fleet of service EV is aimed to serve utility needs. In particular, five EVs, with nominal sizes of 24 kWh and exploitable SOC range of 0.2÷0.9 p.u., are supposed to replace current fuel-based service cars. Their uses are depicted in Figures 2 and 3, in terms of average daily route length and average vehicle parking time, respectively. Each EV leaves the station with a SOC of 0.8 p.u. According to these data, five charging stations are considered in the EVSI since all the EVs are parked at night. It can be noted that EV5 has two parking intervals, therefore they are dealt with separately in the procedure, just as there were six EVs.

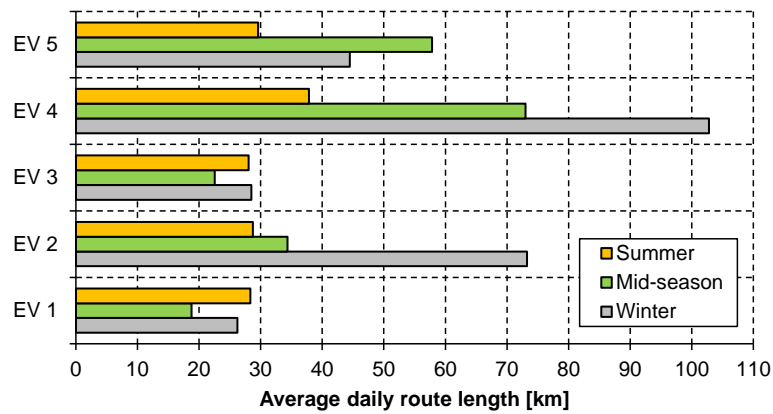


Figure 2. Average route length for the considered vehicle fleet.

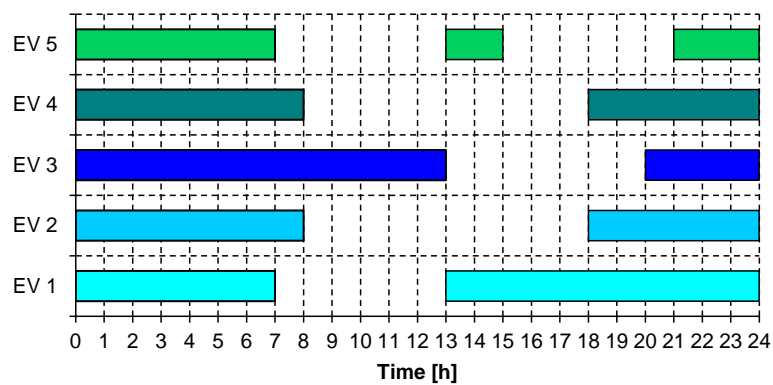


Figure 3. Average parking time for the considered vehicle fleet.

Meteorological data are taken from a one-year measurement of a weather station, on an hourly basis [34]. In accordance with data sources, the analysis is carried out with a time step duration $\Delta t = 1$ h.

The collected data on vehicle usage and weather conditions for the reference year are divided in $N_s = 9$ scenarios, according to seasons and weather conditions, as detailed in Table 1 where the numeration and occurrence times D_s are reported. Within each scenario, a proper ratio of working days and holidays is applied. Two kinds of PV panels and three battery typologies are exploitable, and their features are synthesized in Tables 2 and 3, respectively. Available room for their installation is limited by $S_k = 15 \text{ m}^2$, $S^{tot} = 120 \text{ m}^2$, $V^{tot} = 2 \text{ m}^3$. Moreover, different converter sizes are considered, as reported in Table 4, where efficiency values and installation costs are shown as well. The latter are estimated by proper linear cost functions according to converter size, obtained from an ad hoc market investigation.

Table 1. Scenario numeration and occurrence times.

| Season | Weather Conditions | | | | | |
|------------|--------------------|-------|--------|-------|-------|-------|
| | Sunny | | Cloudy | | Rainy | |
| | Scen. | D_s | Scen. | D_s | Scen. | D_s |
| Winter | 1 | 13 | 2 | 46 | 3 | 31 |
| Mid-season | 4 | 78 | 5 | 69 | 6 | 35 |
| Summer | 7 | 64 | 8 | 25 | 9 | 4 |

Table 2. Photovoltaic (PV) technologies characterization.

| Technology | M_p [kW] | η_p^{std} | c_p [€/kW] |
|-----------------|------------|----------------|--------------|
| Monocrystalline | 0.195 | 0.153 | 1514 |
| Polycrystalline | 0.245 | 0.148 | 1416 |

Table 3. Energy Storage Systems (ESS) technologies characterization.

| Technology | M_i [kWh] | η_i^c, η_i^d | \bar{e}_i, e_{-i} | δ_i | ω_i^c, ω_i^d | z_i [%/h] [35] | c_i [€/kWh] |
|------------|-------------|----------------------|---------------------|------------|--------------------------|------------------|---------------|
| LiPo | 3.7 | 0.95 | 1/0.2 | 561.2 | 0.5/0.5 | 0.020 | 175 |
| ZEBRA | 19.8 | 0.92 | 1/0.2 | 183.0 | 0.66/0.66 | 0.250 | 250 |
| Li-Ion | 2.0 | 0.95 | 1/0.2 | 39.2 | 0.59/0.59 | 0.008 | 300 |

Table 4. Converter technologies features.

| Converter Type | Sizes [kW] | Efficiency [36] | Installation Cost [€] |
|---------------------|----------------|-------------------|--------------------------------------|
| DC/DC monodir. (PV) | 5, 10, 20, 30 | $\zeta^M = 0.975$ | $c_m = 93.247 \cdot W_m + 9531$ |
| DC/DC bidir. (CS) | 10, 20 | $\zeta^K = 0.970$ | $c_r = 86.713 \cdot \Psi_r^c + 7104$ |
| DC/DC bidir. (ESS) | 10, 20, 30, 60 | $\zeta^H = 0.970$ | $c_h = 95.832 \cdot W_i + 9498$ |
| Two-port AC/DC | 10, 20, 30, 60 | $\zeta^F = 0.960$ | $c_f = 41.562 \cdot W_f + 2183$ |

The AC grid connection cost c^g is fixed at 125 €/kWh. The cost of electricity withdrawal from the grid $q_{s,t}^w$ varies for hours and scenarios, in the range $0.14 \div 0.19$ €/kWh, whereas unit revenue for electric energy delivery $\gamma_{s,t}^g$ is in the range $0.025 \div 0.055$ €/kWh [37]. EV charging cost $q_{j,s,t}$ is fixed at 0.05 €/kWh according to values for wearing cost [38], whereas EV discharge is not priced ($\gamma_{j,s,t} = 0$). EVSI lifetime Ny is assumed equal to 20 years, with discount rate α equal to 0.05.

4. Results and Discussion

The procedure is implemented in MatLAB2015b[®] framework, and solved by means of `intlinprog` function. In particular, a first solution of the linear relaxed problem (without integer constraints on variables) is obtained by interior-point, therefore a cut generation to restrict the linear solution is performed and finally the branch-and-bound technique is applied, generating two subproblems by proper heuristics and evaluating the most suitable solution according to best projection on improving lower or upper bounds [39]. Simulations are carried out on a workstation HP Z440 equipped with Intel Xeon 3.50 GHz processor with 16 GB RAM.

In Table 5, the values of average power $\pi_{j,s}$ are synthesized. It can be noted that the values are quite low, seldom exceeding 1 kW, therefore the choice of the minimum size for station is expected.

Table 5. Average power needed to cover electric vehicle (EV) mobility needs [kW].

| EVs | Scenarios | | | | | | | | |
|---------------|-----------|------|------|------|------|------|------|------|------|
| | 1 | 2 | 3 | 4 | 5 | 6 | 7 | 8 | 9 |
| EV1 | 0.10 | 0.13 | 0.08 | 0.07 | 0.08 | 0.07 | 0.11 | 0.12 | 0.09 |
| EV2 | 0.43 | 0.35 | 0.36 | 0.17 | 0.20 | 0.14 | 0.13 | 0.11 | 0.14 |
| EV3 | 0.10 | 0.08 | 0.14 | 0.07 | 0.11 | 0.10 | 0.11 | 0.05 | 0.10 |
| EV4 | 0.47 | 0.46 | 0.55 | 0.28 | 0.45 | 0.36 | 0.17 | 0.21 | 0.23 |
| EV5 (night) | 0.14 | 0.13 | 0.15 | 0.17 | 0.30 | 0.13 | 0.1 | 0.13 | 0.07 |
| EV5 (mid-day) | 0.98 | 0.93 | 1.06 | 1.16 | 2.12 | 0.89 | 0.68 | 0.90 | 0.47 |

As regards EV-station commitment, the results are illustrated in Figure 4. It can be seen that the 5 EVs are associated to stations according to the order of $\pi_{j,s}$, since they are contemporaneously parked

during the night. Moreover, since EV4 always has the maximum power demand, it is always associated with the first station. The mid-day parking interval of EV5 is associated with the first available station.

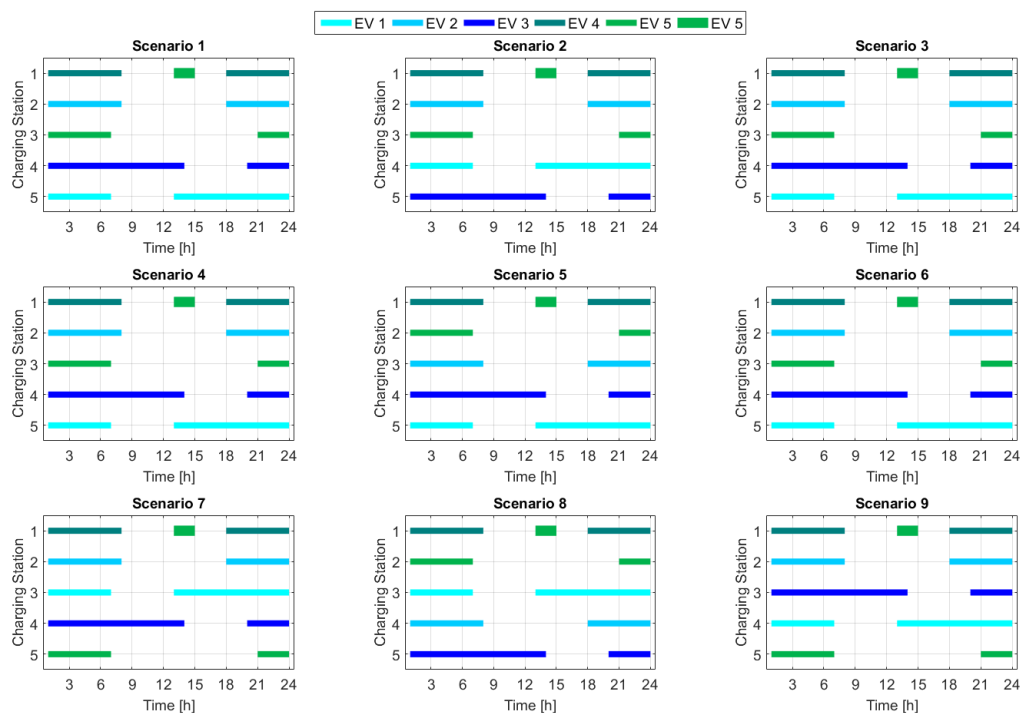


Figure 4. EV-station commitment for each scenario.

A synthesis of the obtained results is reported in Table 6 for installations, where unexploited technologies among the available ones described in Section 2 are not reported for purpose of brevity. It can be seen that the goal of minimum economic effort is reached by exploiting the lower size of EV stations, polycrystalline PV modules and, where deemed necessary, LiPo batteries. No ESS installation is provided, due to the high installation cost of the converter and to the possibility of exploiting EVs for storage tasks thanks to V2G stations.

Table 6. Optimal sizing results: installation sizes.

| Device or Technology | Number | kW | kWh |
|----------------------------|--------|-----------|-----|
| PV polycrystalline modules | 46 | 11.27 | |
| ESS LiPo batteries | 0 | | 0 |
| Bidirectional EV stations | 5 | 10 (each) | |
| Grid connection | 1 | 10 | |
| PV converter | 1 | 20 | |
| ESS converter | 0 | | |
| Two-port grid converter | 1 | 10 | |

Yearly energy exchange levels are reported in Figure 5, where it can be seen that, out of the total value of 19.86 MWh, PV covers 76.1% of production, leaving 16.6% to EV discharge and 7.3% to grid withdrawal. Whereas, total consumption is composed by EV charge for 58.1% grid injection for 35.9% and losses represent 6.0%. Moreover, the ratio of grid withdrawal on grid injection is 0.203, whereas the ratio of EV discharge on EV charge is 0.285, showing a preference to EV as power storage, when present.

Economic results are synthesized in Table 7. It can be noted that the building cost represents almost 93% of the objective function. Operation costs are very limited, reaching 518.5 € yearly.

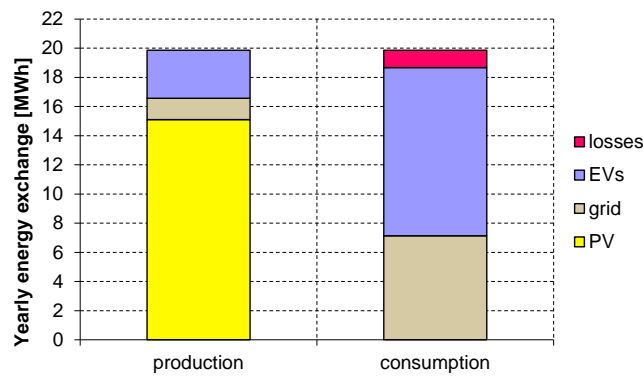


Figure 5. Optimal sizing results: yearly energy exchanges.

Table 7. Optimal sizing results: economic yields.

| Cost Component | Value [€] |
|---------------------------------|-----------|
| Building cost C_B | 83,483.6 |
| Yearly operation cost C_O^Y | 518.5 |
| Lifetime operation cost C_O^Y | 6449.8 |
| Total EVSI cost C_T | 89,933.4 |

For sake of exemplification, trends in all the analyzed scenarios of electric power balance, of EV power exchange levels and of state of charge (SOC) of EVs are reported in Figures 6–8, respectively. It can be seen that an amount of grid power delivery is observed in all scenarios except rainy days of Scenario 3 and Scenario 6, where the limited PV production is fully exploited to charge EVs. Whereas, grid power withdrawal is registered only in five scenarios, and is not present in summer. A limited amount of EV discharge is observed in all scenarios, mostly related to EV 3 and EV 1 due to their parking time in intervals with higher PV production, allowing SOC increase beyond the final value or a decrease towards the minimum. However, EV discharge is present only to exchange power with other EVs.

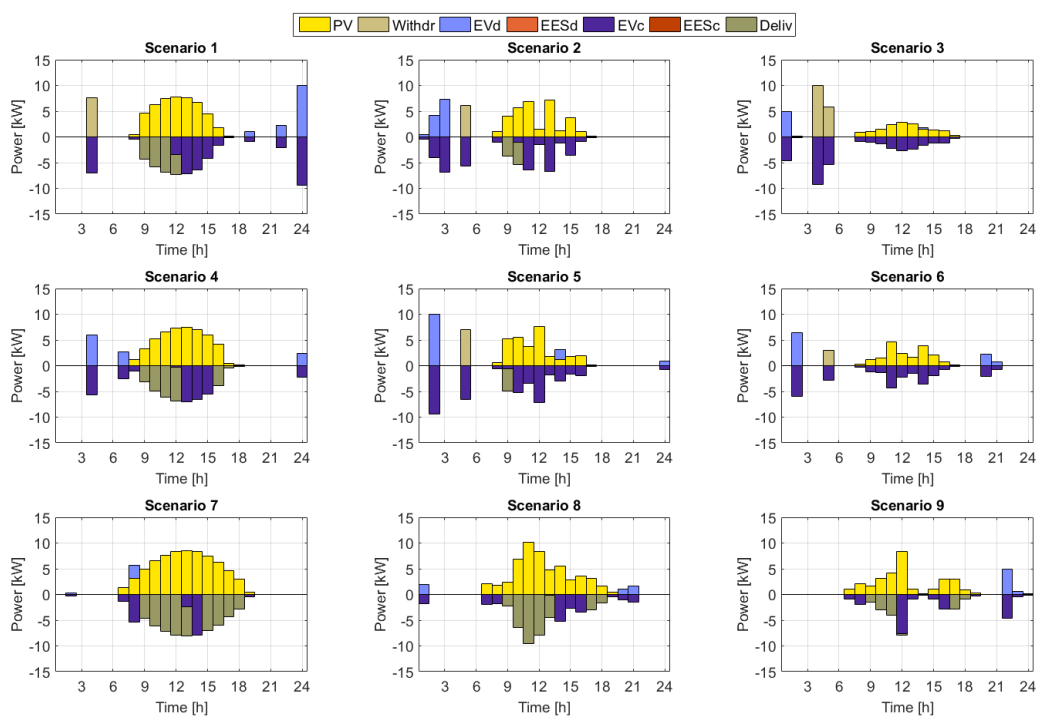


Figure 6. Electric power balance for each scenario.

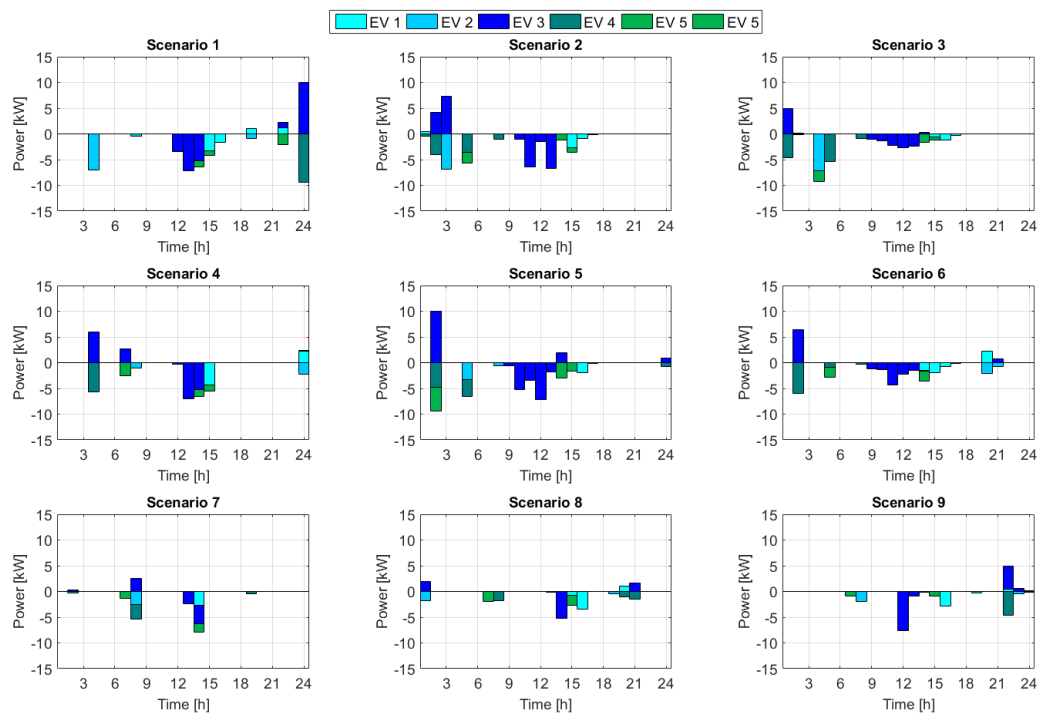


Figure 7. EV power levels for each scenario.

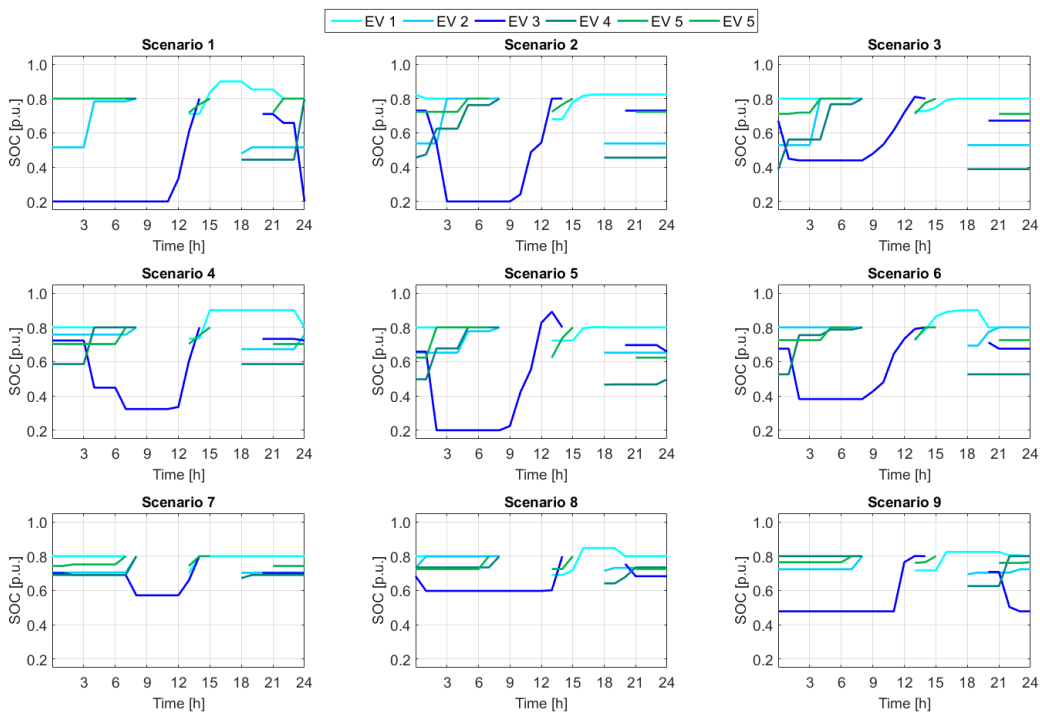


Figure 8. State of charge of EVs for each scenario.

As regards computational performances, the whole procedure took 40.0 s to reach the solution.

5. Conclusions

In this paper, a mixed-integer linear optimization methodology has been carried out for techno-economic sizing of a DC-microgrid including PV canopy, EV charging stations with V2G features, and battery-based ESS with the connection to AC distribution network. The procedure is based on the definition of operating scenarios according to weather conditions and EV uses,

and involves a specific model for the commitment of EV connection to charging station according to EV planned mobility needs. The proposed approach has been applied to a case study of envisaged EV service fleet for Bari Port Authority. Results have shown that the presence of ESS can be hindered by the higher cost due to dedicated converters. The effectiveness of the EV-station commitment strategy has been verified. Future work will deal with the investigation of further DC microgrid configurations, as well as the influence of reliability figures on the selection of the technical solutions.

Author Contributions: M.D., G.F. and R.S. provided for research framework and literature analysis; B.A., G.F. and M.T. developed the model; M.D., I.F. and R.S. cared for data collection; B.A., I.F. and G.F. set up the program and performed the simulations; B.A., I.F. and M.T. formalized the nomenclature; B.A. and G.F. wrote the paper; M.D. and M.T. edited the paper; M.D. and M.T. cared for relation with funding project.

Funding: This document has been created in the context of the CONNECT project. The CONNECT project has received funding from the ECSEL Joint Undertaking under Grant Agreement n° 737434-2 and from the national programmes/funding authorities of Germany, Italy, Slovakia, Spain, and The Netherlands. The ECSEL JU has no liability in respect of this document, which is merely representing the authors' view.

Conflicts of Interest: The authors declare no conflict of interest. The funders had no role in the design of the study; in the collection, analyses, or interpretation of data; in the writing of the manuscript, or in the decision to publish the results.

Nomenclature

Indices (subscripts)

| | |
|-----|--|
| t | Time step |
| s | Scenario |
| p | Photovoltaic (PV) technology |
| i | Energy storage system (ESS) technology |
| j | Electric vehicle (EVs) |
| k | EV station |
| r | Charging/V2G technology standard |
| m | PV converter |
| h | ESS converter |
| f | AC/DC grid connection converter |

Sets and general definitions

| | |
|------------|---|
| Nt | Total number of time steps |
| Ns | Total number of scenarios |
| Ω_p | Set of available PV technologies (total number Np) |
| Ω_i | Set of available ESS technologies (total number Ni) |
| Ω_j | Set of EVs (total number Nj) |
| Ω_k | Set of charging stations (total number Nk) |
| Ω_r | Set of EV charging/V2G standards (total number Nr) |
| Ω_m | Set of PV converters (total number Nm) |
| Ω_h | Set of ESS converters (total number Nh) |
| Ω_f | Set of AC/DC converters (total number Nf) |
| Ny | Total number of years of the analysis |
| α | Discount rate |
| Δt | Duration of each time step [h] |
| D_s | Number of occurrences of the s -th scenario in a year |

Cost breakdown

| | |
|---------|--|
| C_T | Total lifetime cost of the microgrid [€] |
| C_B | Total building cost of the microgrid [€] |
| C_B^P | Building cost of the PVs and their connection [€] |
| C_B^I | Building cost of the ESSs and their connection [€] |
| C_B^K | Building cost of the EV stations and their connection [€] |
| C_B^G | Building cost of DC microgrid internal connections and of AC network interface [€] |
| C_O | Total operation cost of the microgrid [€] |
| C_O^Y | Yearly operation cost of the microgrid [€] |

PV system parameters

| | |
|-------------------|---|
| S_k | parking surface for each charging station [m^2] |
| S^{tot} | total available surface for EV parking roofs [m^2] |
| η_p^{std} | standard efficiency of the p -th PV technology |
| $\eta_{p,s,t}$ | efficiency of the p -th PV technology in the t -th time step of the s -th scenario |
| $G_{p,s,t}$ | solar radiation on the p -th PV at the t -th time step in the s -th scenario [kW/m^2] |
| $\vartheta_{s,t}$ | external temperature at the t -th time step in the s -th scenario [$^{\circ}C$] |
| a_p | power coefficient of the p -th PV technology [$1/K$] |
| ϑ_p | normal operating temperature of the p -th PV technology [$^{\circ}C$] |
| M_p | Unit power of the p -th PV technology panel [kW] |
| W_m | Installed power for the m -th PV converter [kW] |
| ζ^M | PV converter efficiency |
| c_p | Investment cost of a PV panel of the p -th technology [$\text{€}/kW$] |
| c_m | Investment cost of the m -th PV converter [€] |

Energy storage system parameters

| | |
|----------------------------|--|
| η_i^c, η_i^d | charge and efficiency of the i -th ESS |
| \bar{e}_i, e_i | maximum and minimum allowable state of charge SOC for the i -th ESS, in p.u. of installed size |
| $E_{i,s,0}$ | initial condition of SOC for the i -th ESS in the s -th scenario [kWh] |
| V^{tot} | total available volume for hosting ESS [m^3] |
| δ_i | specific energy per unit of volume for the i -th ESS [kWh/m^3] |
| φ_i^c, φ_i^d | energy-to-power ratio, of the i -th ESS in charge and discharge conditions [kWh/kW] |
| z_i | self-discharge rate of the i -th ESS |
| M_i | Unit size of the i -th ESS technology module [kWh] |
| W_h | Installed power for the h -th ESS converter [kW] |
| ζ^H | ESS converter efficiency |
| c_i | Investment cost of an ESS module for the i -th technology [$\text{€}/kWh$] |
| c_h | Investment cost of the h -th ESS converter [€] |

Electric vehicles and stations parameters

| | |
|------------------------------|---|
| ρ_j^c, ρ_j^d | charge and efficiency of the j -th EV |
| \bar{v}_j, v_j | maximum and minimum SOC for the j -th EV |
| $\tau_{j,s}^A, \tau_{j,s}^L$ | arrival and leaving time step of the j -th EV at the station in the s -th scenario |
| $E_{j,s}^A, E_{j,s}^L$ | SOC at arrival and leaving time for the j -th EV in the s -th scenario [kWh] |
| $J_{s,t}$ | number of parked EVs at the t -th time step in the s -th scenario |
| \bar{J}_s | maximum number of parked EVs in the s -th scenario |
| $\bar{\tau}_s$ | time step with the maximum number of parked EVs in the s -th scenario |
| \bar{P}_j^c, \bar{P}_j^d | maximum charge and discharge power of the j -th EV [kW] |
| Ψ_r^c, Ψ_r^d | maximum charge and discharge power of the r -th charging/V2G standard [kW] |
| $\pi_{j,s}$ | Average power needed to charge the j -th EV in the s -th scenario over the defined parking time |
| $\beta_{j,k,s}$ | Binary value assigning the connection of the j -th EV at the k -th station in the s -th scenario |
| ζ^K | charging station efficiency |
| c_r | Investment cost in the r -th technology for vehicle charging/V2G station [€] |
| $q_{j,s,t}, \gamma_{j,s,t}$ | Cost for EV charge and EV discharge at the t -th time step in the s -th scenario [$\text{€}/kWh$] |

Grid connection parameters

| | |
|------------------------------|---|
| W_f | Nominal power of the f -th AC/DC converter [kW] |
| ζ^F | AC/DC converter efficiency |
| $\bar{P}^{\mathcal{S}}$ | Maximum exchangeable power at PCC, in either injection or withdrawal [kW] |
| $q_{s,t}^w$ | Cost for electric energy purchase from the grid at PCC at the t -th time step in the s -th scenario [$\text{€}/kWh$] |
| $\gamma_{s,t}^{\mathcal{S}}$ | Revenue for electric energy delivery to the grid at PCC at the t -th time step in the s -th scenario [$\text{€}/kWh$] |
| c_f | Investment cost of the f -th grid converter [€] |
| $c^{\mathcal{S}}$ | Investment cost of AC grid connection [€] |

Real State Variables

| | |
|---------------|---|
| $P_{s,t}^w$ | Amount of power withdrawal from the distribution grid at the t -th time step in the s -th scenario [kW] |
| $P_{s,t}^g$ | Amount of power injected into the distribution grid at the t -th time step in the s -th scenario [kW] |
| $P_{i,s,t}^c$ | Charge power for the i -th ESS at the t -th time step in the s -th scenario [kW] |
| $P_{i,s,t}^d$ | Discharge power for the i -th ESS at the t -th time step in the s -th scenario [kW] |
| $E_{i,s,t}$ | State of charge (SOC) of the i -th ESS at the t -th time step in the s -th scenario [kWh] |
| $P_{j,s,t}^c$ | Charge power for the j -th EV at the t -th time step in the s -th scenario [kW] |
| $P_{j,s,t}^d$ | Discharge power for the j -th EV at the t -th time step in the s -th scenario [kW] |
| $E_{j,s,t}$ | State of charge (SOC) of the j -th EV at the t -th time step in the s -th scenario [kWh] |
| \bar{P}_k^c | maximum charge power at k -th station |
| \bar{P}_k^d | maximum discharge power at k -th station |
| R_p | Installed power for the p -th PV technology [kW] |
| R_i | Installed size for the i -th ESS technology [kWh] |
| R^F | Installed power for the grid converter [kW] |

Integer State Variables:

| | |
|-------------|--|
| $b_{s,t}^g$ | Variable to select power withdrawal or injection from the AC grid at the t -th time step in the s -th scenario |
| $b_{i,s,t}$ | Variable to select either charge or discharge for the i -th ESS at the t -th time step in the s -th scenario |
| $b_{j,s,t}$ | Variable to select either charge or discharge for the j -th EV at the t -th time step in the s -th scenario |
| $b_{r,k}$ | Variable linking the k -th station to the r -th standard for charging/V2G it is equipped with |
| n_p | Number of modules for the p -th PV technology |
| n_i | Number of battery modules of the i -th ESS technology |
| $b_{m,p}$ | Binary variable indicating if the m -th PV converter is exploited for the p -th PV technology |
| $b_{h,i}$ | Binary variable indicating if the i -th ESS converter is exploited for the i -th ESS technology |
| b_f | Binary variable to select the installation of the f -th two-port AC/DC grid converter |

Appendix A. An Example of EV and Station Commitment Procedure

Let us suppose that a group of 15 EVs should be managed by a microgrid including $Nk=7$ stations, according to a scenario of utilization. In Figure A1, they are numbered according to the power index $\pi_{j,s}$ and their parking times are represented. It can be seen that, in this case, a maximum of $\bar{J}_s = 6$ EVs are contemporaneously parked at $\bar{\tau}_s = 17$, namely, EVs 2, 3, 7, 9, 11, 15. These EVs are associated to the first six stations in this order.

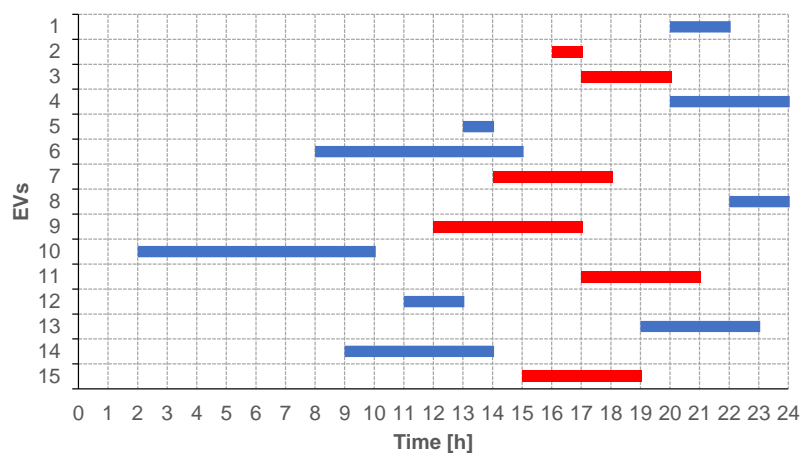


Figure A1. Example of EV and station commitment. Parking time of 15 EVs; in red, the EVs parked at hour 17.

Therefore, the remaining EVs are committed, according to the numbering order. In particular, EV 1 finds station 1 free at its parking time, and is settled there. Whereas, EV 4 cannot be connected to station 1, busy due to the presence of EV 1, nor to station 2, where EV 2 is connected, but it finds station

3 free. Proceeding in this way, the final EV-station commitment is obtained, as reported in Table A1, where bold numbers report EVs parked at hour 17. It can be noted that station 7 is unexploited.

Table A1. Example of EV and station commitment. Allocation of all EVs at microgrid stations.

| hours Stations | 1 | 2 | 3 | 4 | 5 | 6 | 7 | 8 | 9 | 10 | 11 | 12 | 13 | 14 | 15 | 16 | 17 | 18 | 19 | 20 | 21 | 22 | 23 | 24 |
|-------------------|---|----|----|----|----|----|----|----|----|----|----|----|----|----|----|----|----|----|----|----|----|----|----|----|
| 1 | | 10 | 10 | 10 | 10 | 10 | 10 | 10 | 10 | 10 | | | 5 | 5 | | 2 | 2 | | | 1 | 1 | 1 | | |
| 2 | | | | | | | | 6 | 6 | 6 | 6 | 6 | 6 | 6 | 6 | 6 | 3 | 3 | 3 | 3 | | 8 | 8 | 8 |
| 3 | | | | | | | | | | | 12 | 12 | 12 | 7 | 7 | 7 | 7 | 7 | | 4 | 4 | 4 | 4 | 4 |
| 4 | | | | | | | | | | | | 9 | 9 | 9 | 9 | 9 | 9 | | 13 | 13 | 13 | 13 | 13 | |
| 5 | | | | | | | | | 14 | 14 | 14 | 14 | 14 | 14 | | | 11 | 11 | 11 | 11 | 11 | | | |
| 6 | | | | | | | | | | | | | | | 15 | 15 | 15 | 15 | 15 | | | | | |
| 7 | | | | | | | | | | | | | | | | | | | | | | | | |

In this way, for the selected scenario, the binary parameter $\beta_{j,k,s}$ is determined as reported in Table A2, where values equal to 0 are not reported for sake of readability.

Table A2. Example of EV and station commitment. Values of the binary parameter EV-station.

| Stations | EVs | 1 | 2 | 3 | 4 | 5 | 6 | 7 | 8 | 9 | 10 | 11 | 12 | 13 | 14 | 15 |
|----------|-----|---|---|---|---|---|---|---|---|---|----|----|----|----|----|----|
| 1 | | 1 | 1 | | | 1 | | | | | 1 | | | | | |
| 2 | | | | 1 | | | 1 | | 1 | | | | | | | |
| 3 | | | | | 1 | | | 1 | | | | | 1 | | | |
| 4 | | | | | | | | | | 1 | | | | 1 | | |
| 5 | | | | | | | | | | | | 1 | | | 1 | |
| 6 | | | | | | | | | | | | | | | | |
| 7 | | | | | | | | | | | | | | | | 1 |

References

- Vithayasrichareon, P.; Mills, G.; MacGill, I.F. Impact of electric vehicles and solar PV on future generation portfolio investment. *IEEE Trans. Sustain. Energy* **2015**, *6*, 899–908. [\[CrossRef\]](#)
- Schroeder, A.; Traber, T. The economics of fast charging infrastructure for electric vehicles. *Energy Policy* **2012**, *43*, 136–144. [\[CrossRef\]](#)
- Abousleiman, R.; Scholer, R. Smart charging: System design and implementation for interaction between plug-in electric vehicles and the power grid. *IEEE Trans. Transp. Electrification* **2015**, *1*, 18–25. [\[CrossRef\]](#)
- Garcia-Villalobos, J.; Zamora, I.; San Martin, J.I.; Asensio, F.J.; Aperribay, V. Plug-in electric vehicles in electric distribution networks: A review of smart charging approaches. *Renew. Sustain. Energy Rev.* **2014**, *38*, 717–731. [\[CrossRef\]](#)
- You, P.; Yang, Z. Efficient optimal scheduling of charging station with multiple electric vehicles via V2V. In Proceedings of the 2014 IEEE International Conference on Smart Grid Communications, Venice, Italy, 3–6 November 2014; pp. 716–721. [\[CrossRef\]](#)
- Bhatti, R.; Salam, Z.; Aziz, M.J.B.A.; Yee, K.P.; Ashique, R.H. Electric vehicles charging using photovoltaic: Status and technological review. *Renew. Sustain. Energy Rev.* **2016**, *54*, 34–47. [\[CrossRef\]](#)
- Tian, W.; Jiang, W.; Shahidehpour, M.; Krishnamurthy, M. Vehicle charging stations with solar canopy: A realistic case study within a smart grid environment. In Proceedings of the 2014 IEEE Transportation Electrification Conference and Expo, Beijing, China, 31 August–3 September 2014; pp. 1–6. [\[CrossRef\]](#)
- Brenna, M.; Dolara, A.; Foadelli, F.; Leva, S.; Longo, M. Urban scale photovoltaic charging stations for electric vehicles. *IEEE Trans. Sustain. Energy* **2014**, *5*, 1234–1241. [\[CrossRef\]](#)
- Chukwu, U.C.; Mahajan, S.M. V2G parking lot with PV rooftop for capacity enhancement of a distribution system. *IEEE Trans. Sustain. Energy* **2014**, *5*, 119–127. [\[CrossRef\]](#)
- Tulpule, P.J.; Marano, V.; Yurkovich, S.; Rizzoni, G. Economic and environmental impacts of a PV powered workplace parking garage charging station. *Appl. Energy* **2013**, *108*, 323–332. [\[CrossRef\]](#)
- Fattori, F.; Anglani, N.; Muliere, G. Combining photovoltaic energy with electric vehicles, smart charging and vehicle-to-grid. *Solar Energy* **2014**, *110*, 438–451. [\[CrossRef\]](#)

12. Sbordone, D.; Bertini, I.; Di Pietra, B.; Falvo, M.C.; Genovese, A.; Martirano, L. EV fast charging stations and energy storage technologies: A real implementation in the smart micro grid paradigm. *Electr. Power Syst. Res.* **2015**, *120*, 96–108. [[CrossRef](#)]
13. Safak Bayram, I.; Michailidis, G.; Devetsikiotis, M.; Bhattacharya, S.; Chakraborty, A.; Granelli, F. Local energy storage sizing in plug-in hybrid electric vehicle charging stations under blocking probability constraints. In Proceedings of the 2011 IEEE SmartGridComm Conference, Brussels, Belgium, 17–20 October 2011; pp. 78–83. [[CrossRef](#)]
14. Pequito, S.; Popli, N.; Kar, S.; Ilic, M.D.; Aguilar, A.P. A framework for actuator placement in large scale power systems: Minimal strong structural controllability. In Proceedings of the 2013 5th IEEE International Workshop on Computational Advances in Multi-Sensor Adaptive Processing (CAMSAP), St. Martin, France, 15–18 December 2013; pp. 416–419. [[CrossRef](#)]
15. Bruno, S.; La Scala, M.; Stecchi, U. Monitoring and control of a smart distribution network in extended real time DMS framework. In Proceedings of the CIGRE 2011 Bologna Symposium—The Electric Power System of the Future: Integrating Supergrids and Microgrids, Bologna, Italy, 13–15 September 2011. paper 177.
16. Aluisio, B.; Dicorato, M.; Forte, G.; Trovato, M. A Monte-Carlo based procedure for optimal sizing of integrated electric vehicle supply infrastructure. In Proceedings of the IEEE ISGT Europe 2017 Conference, Turin, Italy, 26–29 September 2017; pp. 1–6. [[CrossRef](#)]
17. Aluisio, B.; Dicorato, M.; Ferrini, I.; Forte, G.; Trovato, M. AC and DC solutions for electric vehicle microgrid: Sizing and reliability analysis. In Proceedings of the IEEE 2018 IEEEIC/I&CPS Europe International Conference, Palermo, Italy, 12–15 June 2018; pp. 1–6. [[CrossRef](#)]
18. Chandra Mouli, G.R.; Bauer, P.; Zeman, M. System design for a solar powered electric vehicle charging station for workplaces. *Appl. Energy* **2016**, *168*, 434–443. [[CrossRef](#)]
19. Preetham, G.; Shireen, W. Photovoltaic charging station for plug-in hybrid electric vehicles in a smart grid environment. In Proceedings of the 2012 IEEE PES ISGT Conference, Berlin, Germany, 16–20 January 2012; pp. 1–8. [[CrossRef](#)]
20. Ashique, R.H.; Salam, Z.; Bin Abdul Aziz, M.J.; Bhatti, A.R. Integrated photovoltaic-grid dc fast charging system for electric vehicle: A review of the architecture and control. *Renew. Sustain. Energy Rev.* **2017**, *69*, 1243–1257. [[CrossRef](#)]
21. Kaur, S.; Kaur, T.; Khanna, R.; Singh, P. A state of the art of DC microgrids for electric vehicle charging. In Proceedings of the 4th IEEE ISPC 2k17 Conference, Solan, India, 21–23 September 2017; pp. 381–386. [[CrossRef](#)]
22. Chen, Y.; Wei, W.; Zhang, F.; Liu, C.; Meng, C. Design of PV hybrid DC/AC microgrid for electric vehicle charging station. In Proceedings of the 2017 ITEC Asia-Pacific Conference, Harbin, China, 7–10 August 2017; pp. 1–6. [[CrossRef](#)]
23. Liao, Y.-T.; Lu, C.N. Dispatch of EV charging station energy resources for sustainable mobility. *IEEE Trans. Transp. Electrification* **2015**, *1*, 86–93. [[CrossRef](#)]
24. Tushar, W.; Yuen, C.; Huang, S.; Smith, D.B.; Poor, H.V. Cost minimization of charging stations with photovoltaics: An approach with EV classification. *IEEE Trans. Intell. Transp. Syst.* **2016**, *17*, 156–169. [[CrossRef](#)]
25. Lu, X.; Liu, N.; Chen, Q.; Zhang, J. Multi-objective optimal Scheduling of a DC micro-grid consisted of PV system and EV charging station. In Proceedings of the 2014 IEEE ISGT Asia Conference, Kuala Lumpur, Malaysia, 20–23 May 2014; pp. 487–491. [[CrossRef](#)]
26. Marra, F.; Traeholt, C.; Larsen, E. Planning future electric vehicle central charging station connected to low-voltage distribution network. In Proceedings of the 2012 3rd IEEE International Symposium on Power Electronics for Distributed Generation Systems (PEDG), Aalborg, Denmark, 8 January 2012; pp. 636–641. [[CrossRef](#)]
27. Corchero, C.; Cruz-Zambrano, M.; Heredia, F.-J.; Caro, J.-I.; Igualada-Gonzalez, L.; Romero-Ortega, A. Optimal sizing of microgrid, a fast charging station case. In Proceedings of the 2012 European Energy market (EEM) Conference, Florence, Italy, 10–12 May 2012; pp. 1–6. [[CrossRef](#)]
28. Machiels, N.; Leemput, N.; Van Roy, J.; Geth, F.; Driesen, J. Design criteria for electric vehicle fast charge infrastructure based on Flemish mobility behavior. *IEEE Trans. Smart Grid* **2014**, *5*, 320–327. [[CrossRef](#)]
29. Ugirumurera, J.; Haas, Z.J. Optimal capacity sizing for completely green charging systems for electric vehicles. *IEEE Trans. Transp. Electrification* **2017**, *3*, 565–577. [[CrossRef](#)]

30. Wang, C.; Jiao, B.; Guo, L.; Yuan, K.; Sun, B. Optimal planning of stand-alone microgrids incorporating reliability. *J. Mod. Power Syst. Clean Energy* **2014**, *2*, 195–205. [[CrossRef](#)]
31. Dominguez, E.X.; Arboleya, P. Reliability assessment in photovoltaic nanogrids by means of principal components analysis. In Proceedings of the IEEE 2016 PES General Meeting, Boston, MA, USA, 17–21 July 2016; pp. 1–5. [[CrossRef](#)]
32. Duffie, J.A.; Beckman, W.A. *Solar Engineering of Thermal Processes*, 4th ed.; John Wiley & Sons: Hoboken, NJ, USA, 2013.
33. Zheng, L.; Zhu, J.; Wang, G.; He, T.; Wei, Y. Novel methods for estimating lithium-ion battery state of energy and maximum available energy. *Appl. Energy* **2016**, *178*, 1–8. [[CrossRef](#)]
34. Wunderground—Weather Station Network. Available online: www.wunderground.com (accessed on 1 January 2018).
35. Soloveichik, G.L. Battery technologies for large-scale stationary energy storage. *Annu. Rev. Chem. Biomol. Eng.* **2011**, *2*, 503–527. [[CrossRef](#)]
36. Fathabadi, H. Novel high efficiency DC/DC boost converter for using in photovoltaic systems. *Solar Energy* **2016**, *125*, 22–31. [[CrossRef](#)]
37. ARERA, the Italian Regulatory Authority for Energy, Networks and Environment, Electricity Prices for Customers. Available online: <https://www.arera.it/it/prezzi.htm#> (accessed on 31 October 2018). (In Italian)
38. Aluisio, B.; Conserva, A.; Dicorato, M.; Forte, G.; Trovato, M. Optimal operation planning of V2G-equipped microgrid in the presence of EV aggregator. *Electr. Power Syst. Res.* **2017**, *152*, 295–305. [[CrossRef](#)]
39. Nemhauser, G.L.; Wolsey, L.A. *Integer and Combinatorial Optimization*; John Wiley & Sons: New York, NY, USA, 1999.



© 2019 by the authors. Licensee MDPI, Basel, Switzerland. This article is an open access article distributed under the terms and conditions of the Creative Commons Attribution (CC BY) license (<http://creativecommons.org/licenses/by/4.0/>).